A BODY OF REVOLUTION FINITE DFFERENCE TIME DOMAIN METHOD WITH PERFECTLY MATCHED LAYER ABSORBING BOUNDARY

V. Rodriguez-Pereyra, A. Z. Elsherbeni, and C. E. Smith

Department of Electrical Engineering
The University of Mississippi
University, Mississippi 38677, USA

1. INTRODUCTION

A large number of structures in the field of electromagnetics present symmetry around an axis of rotation. Among these structures there are certain types of transmission media, such as coaxial cables and cylindrical waveguides; and antennas, like wire dipoles, circular microstrip patches, cylindrical dielectric, and resonator antennas. There are also structures that have this rotational symmetry, on to which it is desirable to mount certain electromagnetic device, for example, the fuselage of an aircraft or missile. Since the periodic behavior of the electromagnetic fields around this type of structure is known, it is possible to extract this behavior analytically, and then solve Maxwell's equations on a single two dimensional (2D) plane. This body of revolution (BOR) approach has been applied to several numerical methods in

electromagnetics, including the method of moments (MOM), finite elements method (FEM) and the finite difference time domain (FDTD).

In this paper, a FDTD BOR method is prepared based on the algorithm used in [1, 2] with the added ability to model magnetic materials and magnetic losses. In the algorithm used in [1, 2], the computational domain was terminated with perfect electric conductor (PEC), which limit the method to the study of closed cylindrical cavities. Absorbing boundary conditions (ABC) for the truncation of the mesh for FDTD BOR algorithms have been described in the past. Merewether ABC was used in [3] with a FDTD-BOR algorithm, however this algorithm only took into account a constant variation of the fields in the azimuth (mode 0). The present work introduces Berenger's Perfectly Matched Layer (PML) to the FDTD-BOR algorithm presented in [1, 2]. Even though [4] presented PML on a FDTD BOR code, this was done in such a way that absorption of outgoing waves occurred for waves traveling along the direction of the axis of rotation. That is the case for waveguide-type geometries. In our present work, PML surrounds the computational domain in a way that all outgoing waves are absorbed. The PML may be set to PEC for the analysis of cavity resonators or waveguides. The method has been programmed in such a way that field components are only defined on the computational domain (CD). Similarly PML components are only defined in the surrounding PML layers. This saves large amounts of memory and makes the algorithm very efficient.

2. THE FDTD BOR TECHNIQUE

The FDTD BOR technique is derived starting from Maxwell's curl equations, following the derivation shown in [1, 2] although magnetic materials have been introduced into the equations. The derivation of the updating equations for FDTD BOR starts from Maxwell's curl equations.

$$\nabla \times \vec{E} = -\frac{\partial \mu \vec{H}}{\partial t} + \sigma^m \vec{H}, \quad \text{and} \quad \nabla \times \vec{H} = \frac{\partial \varepsilon \vec{E}}{\partial t} + \sigma^e \vec{E} \quad (1)$$

Where ε is the permittivity, μ is the permeability, σ^e is the electric conductivity, and σ^m is the magnetic conductivity. The electric

properties of the medium are assumed to be in the following form

$$[\alpha] = \begin{bmatrix} \alpha_r & 0 & 0 \\ 0 & \alpha_\varphi & 0 \\ 0 & 0 & \alpha_z \end{bmatrix} \tag{2}$$

where α can be either ε, μ, σ^e, or σ^m. The φ variation of $\boldsymbol{E}$ and $\boldsymbol{H}$ in the cylindrical coordinates system will have the form $\sin(m\varphi)$ or $\cos(m\varphi)$, where m is an integer that represents the mode number. Thus, when applying the curl operators in equation (1) the following terms are obtained

$$\left(\frac{1}{r} \frac{\partial E_z(r, z) \sin(m\varphi)}{\partial \varphi} \right) \hat{a}_r, \text{ and } \left(-\frac{1}{r} \frac{\partial E_r(r, z) \sin(m\varphi)}{\partial \varphi} \right) \hat{a}_z, \text{ or}$$
$$\left(\frac{1}{r} \frac{\partial E_z(r, z) \cos(m\varphi)}{\partial \varphi} \right) \hat{a}_r, \text{ and } \left(-\frac{1}{r} \frac{\partial E_r(r, z) \cos(m\varphi)}{\partial \varphi} \right) \hat{a}_z. \tag{3}$$

by carrying out the derivatives in (3) it yields

$$\left(\frac{1}{r} m E_z(r, z) \cos(m\varphi) \right) \hat{a}_r, \text{ and } \left(-\frac{1}{r} m E_z(r, z) \cos(m\varphi) \right) \hat{a}_z, \text{ or}$$
$$\left(\frac{1}{r}(-m) E_z(r, z) \sin(m\varphi) \right) \hat{a}_r, \text{ and } \left(-\frac{1}{r}(-m) E_z(r, z) \sin(m\varphi) \right) \hat{a}_z. \tag{4}$$

Hence Maxwell's equations in (1) reduce to the following six equations which are given here in a matrix form

$$\begin{bmatrix} 0 & \dfrac{-\partial}{\partial z} & \pm\dfrac{m}{r} \\[2mm] \dfrac{\partial}{\partial z} & 0 & \dfrac{-\partial}{\partial r} \\[2mm] \mp\dfrac{m}{r} & \dfrac{1}{r}\dfrac{\partial r}{\partial r} & 0 \end{bmatrix} \begin{bmatrix} E_r \\[2mm] E_\varphi \\[2mm] E_z \end{bmatrix} = - \begin{bmatrix} \left(\mu_o \mu_r \dfrac{\partial}{\partial t} + \sigma_r^m \right) H_r \\[2mm] \left(\mu_o \mu_\varphi \dfrac{\partial}{\partial t} + \sigma_\varphi^m \right) H_\varphi \\[2mm] \left(\mu_o \mu_z \dfrac{\partial}{\partial t} + \sigma_z^m \right) H_z \end{bmatrix} \tag{5}$$

$$
\begin{bmatrix}
0 & \dfrac{-\partial}{\partial z} & \mp\dfrac{m}{r} \\[2ex]
\dfrac{\partial}{\partial z} & 0 & \dfrac{-\partial}{\partial r} \\[2ex]
\pm\dfrac{m}{r} & \dfrac{1}{r}\dfrac{\partial r}{\partial r} & 0
\end{bmatrix}
\begin{bmatrix} H_r \\[1ex] H_\varphi \\[1ex] H_z \end{bmatrix}
=
\begin{bmatrix}
\left(\varepsilon_o\varepsilon_r\dfrac{\partial}{\partial t} + \sigma_r^e\right)E_r \\[2ex]
\left(\varepsilon_o\varepsilon_\varphi\dfrac{\partial}{\partial t} + \sigma_\varphi^e\right)E_\varphi \\[2ex]
\left(\varepsilon_o\varepsilon_z\dfrac{\partial}{\partial t} + \sigma_z^e\right)E_z
\end{bmatrix}
\tag{6}
$$

Since the change in the φ direction has been removed analytically, the fields at any angle $\varphi = \varphi_o$ can be related to the fields at $\varphi = 0$ and the 3D algorithm is then reduced to 2D in the r-z plane. At this point each equation in (5) and (6) can be discretized by applying finite difference approximations to yield the updating equations for each field component. Starting with the first equation in (6), that is:

$$
\frac{-\partial H_\varphi}{\partial z} - \frac{m}{r}H_z = \varepsilon_o\varepsilon_r\frac{\partial E_r}{\partial t} + \sigma_r^e E_r
\tag{7}
$$

The central difference finite difference approximations are applied and the following equation is obtained

$$
-\left[\frac{H_\varphi^{n+\frac{1}{2}}(i,j) - H_\varphi^{n+\frac{1}{2}}(i,j-1)}{\Delta z}\right] - \frac{m}{r}H_z^{n+\frac{1}{2}}(i,j)
$$
$$
= \varepsilon_o\varepsilon_r\left[\frac{E_r^{n+1}(i,j) - E_r^n(i,j)}{\Delta t}\right] + \sigma_r^e E_r^{n+\frac{1}{2}}(i,j)
\tag{8}
$$

where the superscript n denotes the time index, that is, the time step in the FDTD algorithm, and (i,j) are indexes for the space cell. The index i indicates the position of the cell in the radial direction. Similarly j indicates the position of the cell in the z direction, as shown in Fig. 1. The following average procedure is used for the electric field term at $(n + 1/2)$.

$$
E_r^{n+\frac{1}{2}}(i,j) = \frac{E_r^{n+1}(i,j) + E_r^n(i,j)}{2}
\tag{9}
$$

By introducing (9) into (8), and algebraically collecting the E_r terms, the right hand side (RHS) of (8) may be rewritten as

$$
RHS = \left(\frac{2\varepsilon_o\varepsilon_r + \sigma_r^e\Delta t}{2\Delta t}\right)E_r^{n+1}(i,j) - \left(\frac{2\varepsilon_o\varepsilon_r - \sigma_r^e\Delta t}{2\Delta t}\right)E_r^n(i,j) \tag{10}
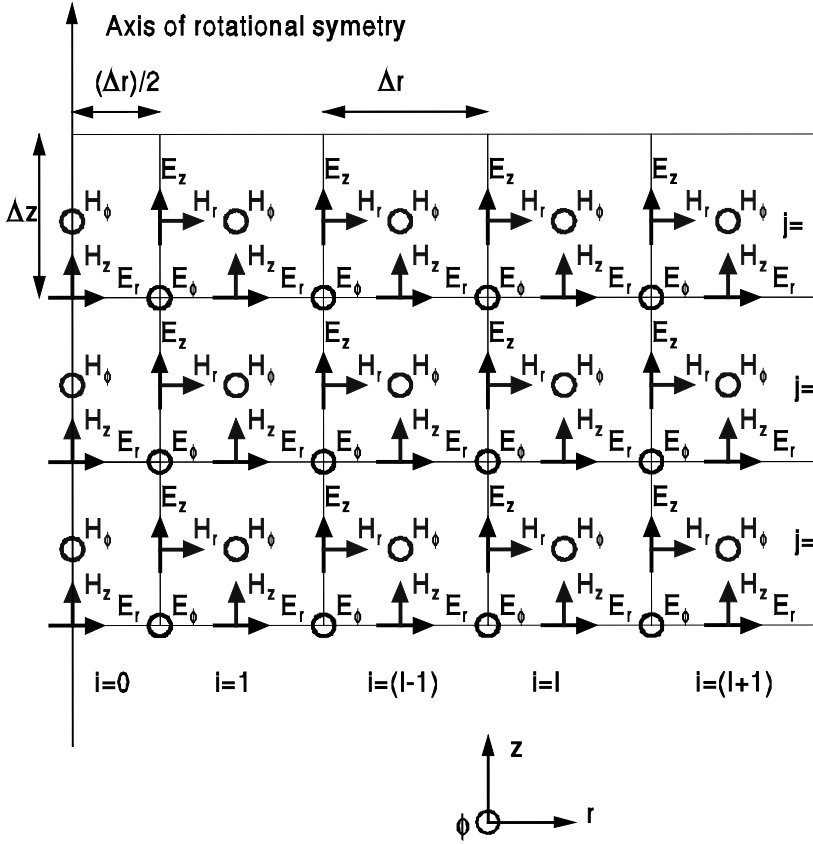$$

Figure 1. A finite difference mesh for BOR-FDTD computations, showing the field components, indexing, cell sizes, and the half cell at the axis.

by combining this with the left hand side (LHS) and rearranging the terms the following updating equation for E_r is obtained

$$E_r^{n+1}(i,j) = \left(\frac{1 - \dfrac{\sigma_r^e \Delta t}{2\varepsilon_o \varepsilon_r}}{1 + \dfrac{\sigma_r^e \Delta t}{2\varepsilon_o \varepsilon_r}} \right) E_r^n(i,j) - \left(\frac{\dfrac{\Delta t}{\varepsilon_o \varepsilon_r}}{1 + \dfrac{\sigma_r^e \Delta t}{2\varepsilon_o \varepsilon_r}} \right)$$

$$\cdot \left[\frac{H_\varphi^{n+\frac{1}{2}}(i,j) - H_\varphi^{n+\frac{1}{2}}(i,j-1)}{\Delta z} - \frac{m H_z^{n+\frac{1}{2}}(i,j)}{(i)\Delta r} \right] \quad (11)$$

which may be written in the following form

$$E_r^{n+1}(i,j) = C_{ere}E_r^n(i,j)$$
$$- C_{erh}\left[\left(\frac{H_\varphi^{n+\frac{1}{2}}(i,j) - H_\varphi^{n+\frac{1}{2}}(i,j-1)}{\Delta z}\right) + \frac{mH_z^{n+\frac{1}{2}}(i,j)}{(i)\Delta r}\right]$$

(12)

Similarly, the other five updating equations are derived and are given here for reference.

$$E_\varphi^{n+1}(i,j) = C_{e\varphi e}E_\varphi^n(i,j)$$
$$+ C_{e\varphi h}\left[\left(\frac{H_r^{n+\frac{1}{2}}(i,j) - H_r^{n+\frac{1}{2}}(i,j-1)}{\Delta z}\right)\right.$$
$$\left. - \left(\frac{H_z^{n+\frac{1}{2}}(i,j) - H_z^{n+\frac{1}{2}}(i-1,j)}{\Delta r}\right)\right]$$

(13)

$$E_z^{n+1}(i,j) = C_{eze}E_z^n(i,j)$$
$$+ C_{ezh}\left[\left(\frac{\Delta r(i)H_\varphi^{n+\frac{1}{2}}(i,j) - \Delta r(i-1)H_\varphi^{n+\frac{1}{2}}(i-1,j)}{\left(i-\frac{1}{2}\right)\Delta r^2}\right)\right.$$
$$\left. + \frac{mH_r^{n+\frac{1}{2}}(i,j)}{\left(i-\frac{1}{2}\right)\Delta r}\right]$$

(14)

$$H_r^{n+\frac{1}{2}}(i,j) = C_{hrh}H_r^{n-\frac{1}{2}}(i,j)$$
$$+ C_{hre}\left[\left(\frac{E_\varphi^n(i,j+1) - E_\varphi^n(i,j)}{\Delta z}\right) - \frac{mE_z^n(i,j)}{\left(i-\frac{1}{2}\right)\Delta r}\right]$$

(15)

$$H_\phi^{n+\frac{1}{2}}(i,j) = C_{h\phi h}H_\phi^{n-\frac{1}{2}}(i,j) - C_{h\phi e}\left[\left(\frac{E_r^n(i,j+1) - E_r^n(i,j)}{\Delta z}\right)\right.$$
$$\left. - \left(\frac{E_z^n(i+1,j) - E_z^n(i,j)}{\Delta r}\right)\right]$$

(16)

$$H_z^{n+\frac{1}{2}}(i,j) = C_{hzh}H_z^{n-\frac{1}{2}}(i,j) + C_{hze}$$

$$\left[-\left(\frac{\left(i+\frac{1}{2}\right)\Delta r E_\varphi^n(i+1,j) - \left(i-\frac{1}{2}\right)\Delta r E_\varphi^n(i,j)}{(i)\Delta r^2} \right) \right.$$

$$\left. + \frac{mE_r^n(i,j)}{(i)\Delta r} \right] \tag{17}$$

Where the coefficients in these update equations are shown below

$$C_{ere} = \left(\frac{1 - \dfrac{\sigma_r^e \Delta t}{2\varepsilon_o \varepsilon_r}}{1 + \dfrac{\sigma_r^e \Delta t}{2\varepsilon_o \varepsilon_r}} \right), \ C_{erh} = \left(\frac{\dfrac{\Delta t}{\varepsilon_o \varepsilon_r}}{1 + \dfrac{\sigma_r^e \Delta t}{2\varepsilon_o \varepsilon_r}} \right), \ C_{e\varphi e} = \left(\frac{1 - \dfrac{\sigma_\varphi^e \Delta t}{2\varepsilon_o \varepsilon_\varphi}}{1 + \dfrac{\sigma_\varphi^e \Delta t}{2\varepsilon_o \varepsilon_\varphi}} \right)$$

$$C_{e\varphi e} = \left(\frac{\dfrac{\Delta t}{\varepsilon_o \varepsilon_\varphi}}{1 + \dfrac{\sigma_\varphi^e \Delta t}{2\varepsilon_o \varepsilon_\varphi}} \right), \ C_{eze} = \left(\frac{1 - \dfrac{\sigma_z^e \Delta t}{2\varepsilon_o \varepsilon_z}}{1 + \dfrac{\sigma_z^e \Delta t}{2\varepsilon_o \varepsilon_z}} \right), \ C_{ezh} = \left(\frac{\dfrac{\Delta t}{\varepsilon_o \varepsilon_z}}{1 + \dfrac{\sigma_z^e \Delta t}{2\varepsilon_o \varepsilon_z}} \right) \tag{18}$$

and

$$C_{hrh} = \left(\frac{1 + \dfrac{\sigma_r^m \Delta t}{2\mu_o \mu_r}}{1 - \dfrac{\sigma_r^m \Delta t}{2\mu_o \mu_r}} \right), \ C_{hre} = \left(\frac{\dfrac{\Delta t}{\mu_o \mu_r}}{1 - \dfrac{\sigma_r^m \Delta t}{2\mu_o \mu_r}} \right), \ C_{h\varphi h} = \left(\frac{1 + \dfrac{\sigma_\varphi^m \Delta t}{2\mu_o \mu_\varphi}}{1 - \dfrac{\sigma_\varphi^m \Delta t}{2\mu_o \mu_\varphi}} \right)$$

$$C_{h\varphi e} = \left(\frac{\dfrac{\Delta t}{\mu_o \mu_\varphi}}{1 - \dfrac{\sigma_\varphi^m \Delta t}{2\mu_o \mu_\varphi}} \right), \ C_{hzh} = \left(\frac{1 + \dfrac{\sigma_z^m \Delta t}{2\mu_o \mu_z}}{1 - \dfrac{\sigma_z^m \Delta t}{2\mu_o \mu_z}} \right), \ C_{hze} = \left(\frac{\dfrac{\Delta t}{\mu_o \mu_z}}{1 + \dfrac{\sigma_z^m \Delta t}{2\mu_o \mu_z}} \right) \tag{19}$$

From the equations above it is clear that singularities occur for $r = 0$, that is, at the cells with indexes $(0,j)$. The singularity at the axis is handled in the same manner as in [1, 2]. Using a half cell at the axis (cell of index $i = 0$) makes H_z the only axis component that is needed to update the fields on adjacent cells, and only when $m = 0$. The H_z component may be updated by using Faraday's law:

$$\oint_{\Delta c} \vec{E} \cdot d\vec{l} = -\iint_{\Delta s} \mu \frac{\partial \vec{H}}{\partial t} \cdot d\vec{s} - \iint_{\Delta s} \sigma^m \vec{H} \cdot d\vec{s} \tag{20}$$

The updating equation for the axis H_z component is then given by

$$H_z^{n+\frac{1}{2}}(0,j) = \frac{-4}{\Delta r \left(\Delta t \sigma_z^m + 2\mu_o \mu_z \right)} E_\varphi^n(1,j)$$
$$- \left(\frac{\Delta t \sigma_z^m - 2\mu_o \mu_z}{\Delta t \sigma_z^m + 2\mu_o \mu_z} \right) H_z^{n-\frac{1}{2}}(0,j) \qquad (21)$$

The updating equations (12–17) and (21) are used in the computational domain (CD). Surrounding the CD except for the axis of rotation, an absorbing boundary condition (ABC) is created on the PML algorithm.

3. THE PML BOR ABC

The PML ABC introduced in [5] is used in the present work to absorb outgoing waves and avoid undesired reflections due to the truncation of the mesh. As in the normal FDTD-BOR algorithm, the update equations for the PML surrounding region start from Maxwell's curl equations assuming isotropic media. The basic concept of the PML method is to split the components in two. The reason for doing this is to break any incident wave into two propagating waves that propagate in directions normal to each other. Only the normal incident wave is absorbed in a given PLM region, except for the corners. Figure 2 shows how an incident wave is absorbed in the PML ABC.

A total of twelve split field equations are obtained from the six equations in (5) and (6)

$$\frac{\partial \left(E_{\varphi z} + E_{\varphi r} \right)}{\partial z} = \mu \frac{\partial H_{rz}}{\partial t} + \sigma_z^m H_{rz},$$
$$\mp \frac{m}{r} \left(E_{zr} + E_{z\varphi} \right) = \mu \frac{\partial H_{r\varphi}}{\partial t} + \sigma_\varphi^m H_{r\varphi} \qquad (22)$$

$$\frac{\partial \left(E_{zr} + E_{z\varphi} \right)}{\partial r} = \mu \frac{\partial H_{\varphi r}}{\partial t} + \sigma_r^m H_{\varphi r},$$
$$-\frac{\partial \left(E_{rz} + E_{r\varphi} \right)}{\partial z} = \mu \frac{\partial H_{\varphi z}}{\partial t} + \sigma_z^m H_{\varphi z} \qquad (23)$$

$$-\frac{1}{r} \frac{\partial r \left(E_{\varphi z} + E_{\varphi r} \right)}{\partial r} = \mu \frac{\partial H_{zr}}{\partial t} + \sigma_r^m H_{zr},$$
$$\frac{m}{r} \left(E_{rz} + E_{r\varphi} \right) = \mu \frac{\partial H_{z\varphi}}{\partial t} + \sigma_\varphi^m H_{z\varphi} \qquad (24)$$
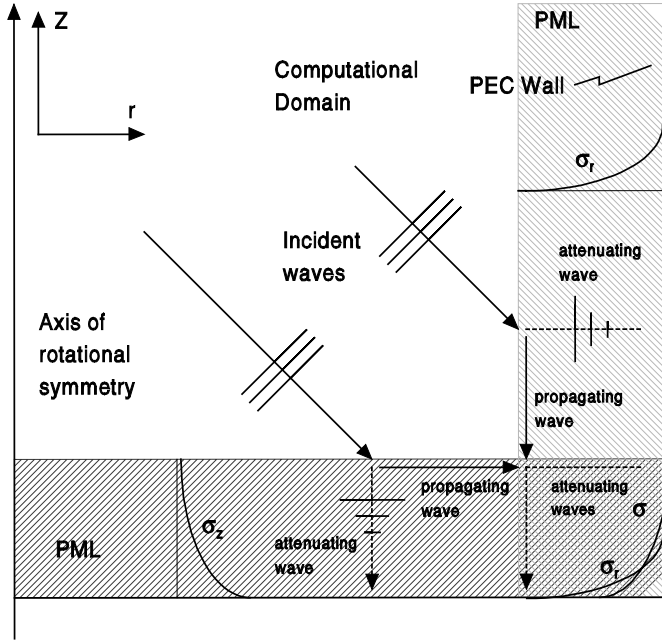
Figure 2. Absorption at the PML Region.

$$-\frac{\partial\left(H_{\varphi z}+H_{\varphi r}\right)}{\partial z}=\varepsilon\frac{\partial E_{rz}}{\partial t}+\sigma_z^e E_{rz},$$

$$\pm\frac{m}{r}\left(H_{zr}+H_{z\varphi}\right)=\varepsilon\frac{\partial E_{r\varphi}}{\partial t}+\sigma_\varphi^e E_{r\varphi} \tag{25}$$

$$-\frac{1}{r}\frac{\partial r\left(H_{\varphi z}+H_{\varphi r}\right)}{\partial r}=\varepsilon\frac{\partial E_{zr}}{\partial t}+\sigma_r^e E_{zr},$$

$$\frac{m}{r}\left(H_{rz}+H_{r\varphi}\right)=\varepsilon\frac{\partial E_{z\varphi}}{\partial t}+\sigma_\varphi^e E_{z\varphi} \tag{26}$$

and

$$-\frac{\partial\left(H_{zr}+H_{z\varphi}\right)}{\partial r}=\varepsilon\frac{\partial E_{\varphi r}}{\partial t}+\sigma_r^e E_{\varphi r},$$

$$\frac{\partial\left(H_{rz}+H_{r\varphi}\right)}{\partial z}=\varepsilon\frac{\partial E_{\varphi z}}{\partial t}+\sigma_z^e E_{\varphi z} \tag{27}$$

To each of these equations, the same finite difference approximations and averaging for conductivity terms that were used in deriving the CD FDTD-BOR are applied. Each equation then gives an updating equation for one of the twelve split components.

The electric field PML equations are written as

$$E_{rz}^{n+1}(i,j) = -C_{erze}E_{rz}^n(i,j) + C_{erzh}\frac{1}{\Delta z}\left(H_{\varphi z}^{n+\frac{1}{2}}(i,j) - H_{\varphi z}^{n+\frac{1}{2}}(i,j-1)\right.$$

$$\left. + H_{\varphi r}^{n+\frac{1}{2}}(i,j) - H_{\varphi r}^{n+\frac{1}{2}}(i,j-1)\right) \tag{28}$$

$$E_{r\varphi}^{n+1}(i,j) = -C_{er\varphi e}E_{r\varphi}^n(i,j)$$

$$+ C_{er\varphi h}\frac{m}{(i)\Delta r}\left(H_{zr}^{n+\frac{1}{2}}(i,j) + H_{z\varphi}^{n+\frac{1}{2}}(i,j)\right) \tag{29}$$

$$E_{\varphi r}^{n+1}(i,j) = -C_{e\varphi re}E_{\varphi r}^n(i,j) - C_{e\varphi rh}\frac{1}{\Delta r}\left(H_{zr}^{n+\frac{1}{2}}(i,j) - H_{zr}^{n+\frac{1}{2}}(i-1,j)\right.$$

$$\left. + H_{z\varphi}^{n+\frac{1}{2}}(i,j) - H_{z\varphi}^{n+\frac{1}{2}}(i-1,j)\right) \tag{30}$$

$$E_{\varphi z}^{n+1}(i,j) = -C_{e\varphi ze}E_{\varphi z}^n(i,j) + C_{e\varphi zh}\frac{1}{\Delta z}\left(H_{rz}^{n+\frac{1}{2}}(i,j) - H_{rz}^{n+\frac{1}{2}}(i,j-1)\right.$$

$$\left. + H_{r\varphi}^{n+\frac{1}{2}}(i,j) - H_{r\varphi}^{n+\frac{1}{2}}(i,j-1)\right) \tag{31}$$

$$E_{zr}^{n+1}(i,j) = -C_{ezre}E_{zr}^n(i,j) - C_{ezrh}\frac{1}{\left(i-\frac{1}{2}\right)\Delta r^2}\left((i)\Delta r H_{\varphi z}^{n+\frac{1}{2}}(i,j)\right.$$

$$- (i-1)\Delta r H_{\varphi z}^{n-\frac{1}{2}}(i-1,j) + (i)\Delta r H_{\varphi r}^{n+\frac{1}{2}}(i,j)$$

$$\left. -(i-1)\Delta r H_{\varphi r}^{n+\frac{1}{2}}(i-1,j)\right) \tag{32}$$

$$E_{z\varphi}^{n+1}(i,j) = -C_{ez\varphi e}E_{z\varphi}^n(i,j)$$

$$+ C_{ez\varphi h}\frac{m}{\left(i-\frac{1}{2}\right)\Delta r}\left(H_{rz}^{n+\frac{1}{2}}(i,j) + H_{r\varphi}^{n+\frac{1}{2}}(i,j)\right) \tag{33}$$

where

$$C_{e\varphi re} = C_{ezre} = \left(\frac{\sigma_r^e\Delta t - 2\varepsilon}{\sigma_r^e\Delta t + 2\varepsilon}\right), \quad C_{e\varphi rh} = C_{ezrh} = \left(\frac{2\Delta t}{\sigma_r^e\Delta t + 2\varepsilon}\right),$$

$$C_{er\varphi e} = C_{ez\varphi e} = \left(\frac{\sigma_\varphi^e\Delta t - 2\varepsilon}{\sigma_\varphi^e\Delta t + 2\varepsilon}\right), \quad C_{er\varphi h} = C_{ez\varphi h} = \left(\frac{2\Delta t}{\sigma_\varphi^e\Delta t + 2\varepsilon}\right),$$

$$C_{erze} = C_{e\varphi ze} = \left(\frac{\sigma_z^e\Delta t - 2\varepsilon}{\sigma_z^e\Delta t + 2\varepsilon}\right), \quad C_{erzh} = C_{e\varphi zh} = \left(\frac{2\Delta t}{\sigma_\varphi^e\Delta t + 2\varepsilon}\right),$$

$$\tag{34}$$

and the Magnetic field equations are

$$
\begin{aligned}
H_{rz}^{n+\frac{1}{2}}(i,j) = & -C_{hrzh}H_{rz}^{n-\frac{1}{2}}(i,j) + C_{hrze}\frac{1}{\Delta z}\left(E_{\varphi z}^n(i,j+1)\right. \\
& \left. -E_{\varphi z}^n(i,j) + E_{\varphi r}^n(i,j+1) - E_{\varphi r}^n(i,j)\right)
\end{aligned} \tag{35}
$$

$$
\begin{aligned}
H_{r\varphi}^{n+\frac{1}{2}}(i,j) = & -C_{hr\varphi h}H_{r\varphi}^{n-\frac{1}{2}}(i,j) \\
& +C_{hr\varphi e}\frac{m}{\left(i-\frac{1}{2}\right)\Delta r}\left(E_{zr}^n(i,j)+E_{z\varphi}^n(i,j)\right)
\end{aligned} \tag{36}
$$

$$
\begin{aligned}
H_{\varphi r}^{n+\frac{1}{2}}(i,j) = & -C_{h\varphi rh}H_{\varphi r}^{n-\frac{1}{2}}(i,j) + C_{h\varphi rh}\frac{1}{\Delta r}\left(E_{zr}^n(i+1,j)\right. \\
& \left. -E_{zr}^n(i,j) + E_{z\varphi}^n(i+1,j) - E_{z\varphi}^n(i,j)\right)
\end{aligned} \tag{37}
$$

$$
\begin{aligned}
H_{\varphi z}^{n+\frac{1}{2}}(i,j) = & -C_{h\varphi zh}H_{\varphi z}^{n-\frac{1}{2}}(i,j) - C_{h\varphi ze}\frac{1}{\Delta z}\left(E_{rz}^n(i,j+1)\right. \\
& \left. -E_{rz}^n(i,j) + E_{r\varphi}^n(i,j+1) - E_{r\varphi}^n(i,j)\right)
\end{aligned} \tag{38}
$$

$$
\begin{aligned}
H_{zr}^{n+\frac{1}{2}}(i,j) = & -C_{hzrh}H_{zr}^{n-\frac{1}{2}}(i,j) - C_{hz\varphi e}\frac{1}{(i)\Delta r^2} \\
& \cdot\left(\left(i+\frac{1}{2}\right)\Delta r E_{\varphi z}^n(i+1,j) - \left(i-\frac{1}{2}\right)\Delta r E_{\varphi z}^n(i,j)\right. \\
& \left. +\left(i+\frac{1}{2}\right)\Delta r E_{\varphi r}^n(i+1,j) - \left(i-\frac{1}{2}\right)\Delta r E_{\varphi r}^n(i,j)\right)
\end{aligned} \tag{39}
$$

$$
\begin{aligned}
H_{z\varphi}^{n+\frac{1}{2}}(i,j) = & -C_{hz\varphi h}H_{z\varphi}^{n-\frac{1}{2}}(i,j) \\
& +C_{hz\varphi e}\frac{m}{(i)\Delta r}\left(E_{rz}^n(i,j)+E_{r\varphi}^n(i,j)\right)
\end{aligned} \tag{40}
$$

where

$$
\begin{aligned}
C_{hzrh} = C_{h\varphi rh} &= \left(\frac{\sigma_r^m\Delta t - 2\mu}{\sigma_r^m\Delta t + 2\mu}\right), \ C_{hzre} = C_{h\varphi re} = \left(\frac{2\Delta t}{\sigma_r^m\Delta t + 2\mu}\right), \\
C_{hr\varphi h} = C_{hz\varphi h} &= \left(\frac{\sigma_\varphi^m\Delta t - 2\mu}{\sigma_\varphi^m\Delta t + 2\mu}\right), \ C_{hr\varphi e} = C_{hz\varphi e} = \left(\frac{2\Delta t}{\sigma_\varphi^m\Delta t + 2\mu}\right), \\
C_{hrzh} = C_{h\varphi zh} &= \left(\frac{\sigma_z^m\Delta t - 2\mu}{\sigma_z^m\Delta t + 2\mu}\right), \ C_{hrze} = C_{h\varphi ze} = \left(\frac{2\Delta t}{\sigma_z^m\Delta t + 2\mu}\right),
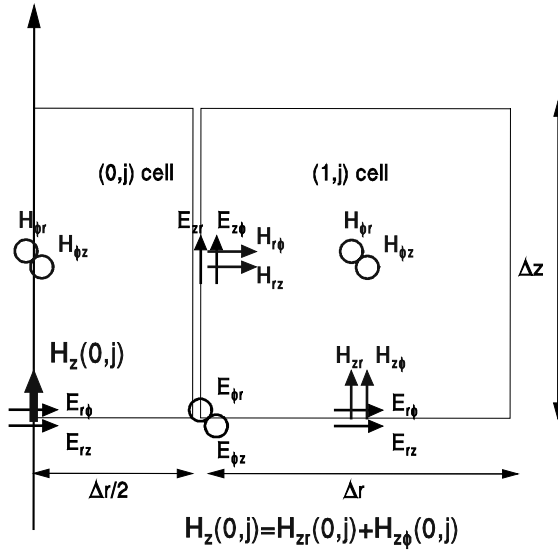\end{aligned} \tag{41}
$$

Figure 3. The PML region close to the axis of rotational symmetry.

As was the case with the CD updating equations, a special equation is needed to take care of the singularities that appear at the axis. At the axis half cell, a total of six PML components are present, as shown in Fig. 3. These components are $H_{\varphi r}$, $H_{\varphi z}$, $E_{r\varphi}$, E_{rz}, H_{zr}, and $H_{z\varphi}$, all of them with indexes $(0, j)$. From the update equations above, it is found that to update $E_{zr}(1, j)$, both $H_{\varphi r}(0, j)$, and $H_{\varphi z}(0, j)$ are needed, but these components are being multiplied by $r(0)$ which is zero, hence they are not needed for updating $E_{zr}(1, j)$.

A study of the update equations reveals that the only non-axis component that is being updated using axis components is $E_{\varphi r}(1, j)$. If the $E_{\varphi r}(1, j)$ update equation is re-written for the special case $i = 1$, after rearranging the terms, we get

$$E_{\varphi r}^{n+1}(1, j) = - \left(\frac{\sigma_r^e \Delta t - 2\varepsilon}{\sigma_r^e \Delta t + 2\varepsilon} \right) E_{\varphi r}^n(1, j) - \left(\frac{2\Delta t}{(\sigma_r^e \Delta t + 2\varepsilon)\, \Delta r} \right)$$

$$\cdot \left(H_{zr}^{n+\frac{1}{2}}(1, j) + H_{z\varphi}^{n+\frac{1}{2}}(1, j) - \left[H_{zr}^{n+\frac{1}{2}}(0, j) + H_{z\varphi}^{n+\frac{1}{2}}(0, j) \right] \right)$$

$$(42)$$

using the fact that

$$H_{zr} + H_{z\varphi} = H_z \tag{43}$$

we rewrite (42) as

$$
\begin{aligned}
E_{\varphi r}^{n+1}(1,j) = {}& - \left(\frac{\sigma_r^e \Delta t - 2\varepsilon}{\sigma_r^e \Delta t + 2\varepsilon} \right) E_{\varphi r}^n(1,j) - \left(\frac{2\Delta t}{(\sigma_r^e \Delta t + 2\varepsilon)\,\Delta r} \right) \\
& \cdot \left(H_{zr}^{n+\frac{1}{2}}(1,j) + H_{z\varphi}^{n+\frac{1}{2}}(1,j) - \left[(H_z^{n+\frac{1}{2}}(0,j) \right] \right)
\end{aligned} \tag{44}
$$

So at the axis it is only necessary to compute the non-split H_z, which may be done by using the integral form of Maxwell's equation. Therefore, $E_{r\varphi}(0,j)$ and $E_{rz}(0,j)$ are not needed to update $H_{z\varphi}(0,j)$.

Following the derivation for $H_z(0,j)$ presented for the CD components, the update equation for $H_z(0,j)$ in the PML region is derived. Notice at this point, that in the PML region, of the φ directed components of the electric field: $E_{\varphi r}$ and $E_{\varphi z}$, only $E_{\varphi r}$ is related to H_{zr}, and $H_{z\varphi}$. Thus when performing Faraday's Law only $E_{\varphi r}$ is used, yielding

$$H_z^{n+\frac{1}{2}}(0,j) = H_z^{n-\frac{1}{2}}(0,j) - \frac{2\Delta t}{2\mu \Delta r} \left(E_{\varphi r}^n(1,j) + E_{\varphi z}^n(1,j) \right) \tag{45}$$

The profile of the magnetic and electric conductivities in the PML region is obtained by using the approach presented in [5], where the electric and magnetic losses follow the following condition for reflectionless layers,

$$\frac{\sigma_\xi^m}{\mu} = \frac{\sigma_\xi^e}{\varepsilon}, \quad \text{where } \xi = r \text{ or } z. \tag{46}$$

where ε and μ are the CD medium permeability and permittivity.

These losses increase from zero at the PML-CD boundary to a maximum value at the last PML layer following a parabolic profile, as an example, as described in [5].
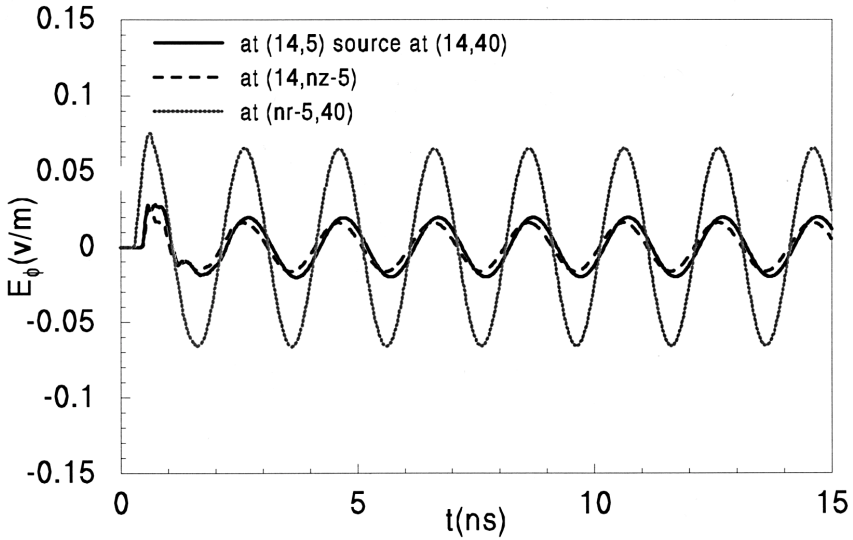
source, $E\phi r + E\phi z = \sin(2\pi\,.5\mathrm{x}10^9 t)$

Figure 4. The E_φ field sampled at points 5 cells away from the lossy PML.

4. NUMERICAL RESULTS

4.1 Verification of the PML equations

To verify that the derived PML equations and algorithm gives correct results, a computational domain ($nr = 52$, $nz = 102$) full of PML updating equations was prepared first. The losses were set to zero except on the outer 10 cells, where they were set following the parabolic profile approach with σ^e_{max} computed based on the value of the theoretical reflection at normal incidence $R(0)$ being 10^{-8} as given in [5]. This value of $R(0)$ is used in all examples presented in this paper. The E_φ component was set to have a sine waveform behavior at node (14,40). Figure 4 shows the E_φ field sampled a few cells from the active PML specifically at (14,5), (14,75), and (37,40). Apart from a small distortion due to the "turn on" of the source, no reflection is apparent from the mesh truncation using the lossy PML region.
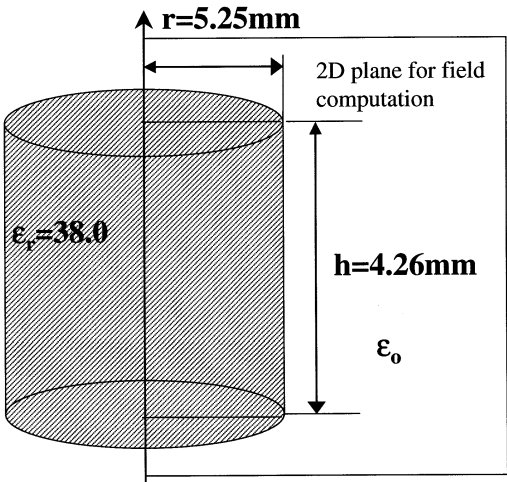
Figure 5. Geometry of the dielectric resonator in free space.

Mode	Experimental [6]	FDTD-BOR-PML	% error
TE01	4.85	4.92	2.06
HEM12	6.64	6.6	0.6
TM01	7.6	7.62	0.2
HEM21	7.81	7.9	1.15
Mode	Computed [6]	FDTD-BOR-PML	% error
HEM11	6.3	6.45	2.3
HEM22	8.455	8.45	0.06
TE03	9.10	9.15	0.55
HEM13	9.35	9.42	0.75
HEM14	9.92	10.	0.80

Table 1. Resonant frequencies (GHz) of the dielectric resonator, compared with previously published data.
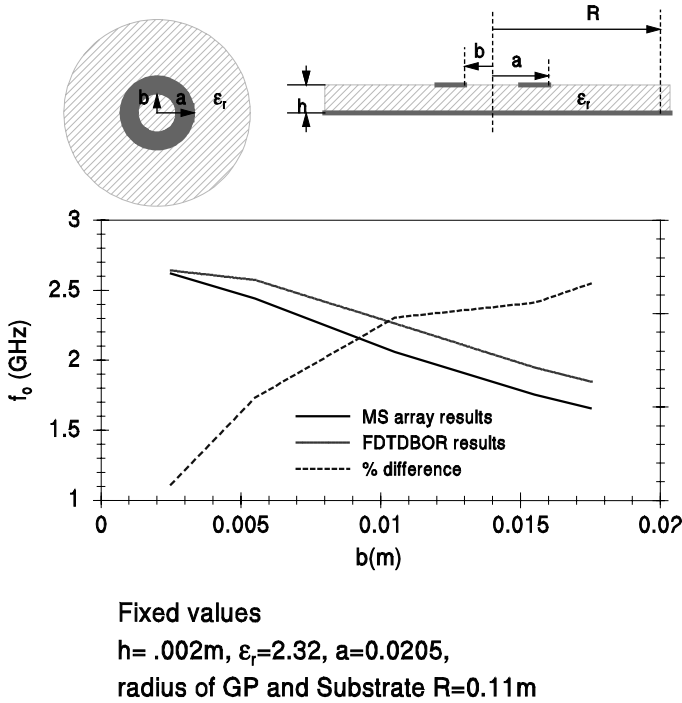
Figure 6. Effects of the inner radius on the resonance of an annular microstrip antenna.

4.2 Applications

a. *Dielectric resonator in free space*

The dielectric resonator studied in [6] is analyzed here, and the computed resonant frequencies are compared with the previously published results. The geometry is a cylindrical resonator of radius $r = 5.25$ mm and a height $h = 4.26$ mm, as shown on Fig. 5. Table 1 shows the resonant frequencies computed with the FDTD-BOR with surrounding PML compared with the results published in [6].

b. *Printed microstrip annular patch antenna*

The operating frequencies of an annular microstrip antenna were computed using the developed code. The effects of changing the inner radius on the resonant frequency of the TM_{11} mode was the core of this study. The results from the FDTD-BOR code with PML were

compared with the results from the MS-Arrays program [7], as shown in Fig. 6. The MS-Arrays code uses the cavity model approximation, which could explain the difference between the results obtained with the two methods since the FDTD-BOR model did not include an infinite ground plane. The dimensions used in our simulation are as follows: $a = 0.0205$ m; $h = 0.002$ m; $\varepsilon_r = 2.32$; the radius of the ground $R = 0.11$ m. The cell sizes are $\Delta z = \Delta r = 1.0$ mm, the number of cells in the CD in the r and z directions are $nr = 110$, $nz = 20$, and the number of PML layers is $nl = 10$, the simulation ran for 30,000 time steps.

c. *Printed microstrip circular patch antenna*

A microstrip patch of radius (a) on a finite grounded substrate was analyzed. Results for this geometry appeared in [8]. The radius a is changed from 0.5 to 0.9 cm. The ground plane is finite, with $R = 26.25$ mm, h is set to 0.0795 mm with $\varepsilon_r = 2.35$, $\Delta z = 0.03975$ cm, $\Delta r = 0.04$ cm, $nr = 658$, $nz = 70$, $nl = 10$, and 30000 steps. Results from the MOM, the cavity model approximation, the MS-Arrays program and the FDTD- BOR are shown on Fig. 7. A very good agreement between all the methods is seen, these agreement tends to be worse as the frequency of resonance increases. For $a = 0.5$ cm there is no good agreement between the FDTD and the other methods, even when the cell size was reduced to take into account the higher frequencies. This case is presently under investigation.

d. *A tapered cavity for the measurement of liquids dielectric constant*

The FDTD-BOR-PML code was used to analyze a cavity used for the measurement of the properties of liquids. This case shows that the PML may be set to PEC to analyze closed cavities and waveguides. The cavity was designed so that no electromagnetic energy will propagate out of it through the pipes used for the liquid to flow. The cavity was analyzed with the pipes shorted and matched. The matching was accomplished by extending the pipes to the PML, as shown on Fig. 8. Figure 9 shows the field inside the cavity at a given time step, the figure illustrate that the geometry was correctly defined, including the staircase approximation to the 45 degree tapered ends. Figure 10 shows the results after performing Fourier transform on the time domain data. The field is sampled next to the excitation probe. The first resonance (TM11) at 15.7 GHz matches with the measurements. Also it is noticed that no difference exists between the shorted ends and the
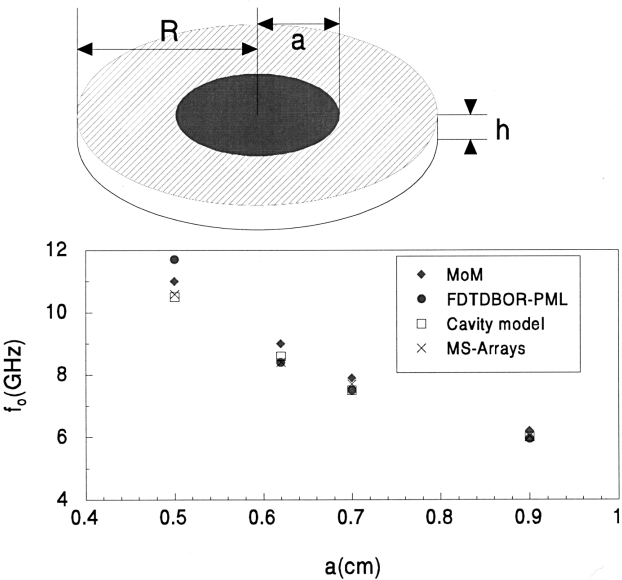
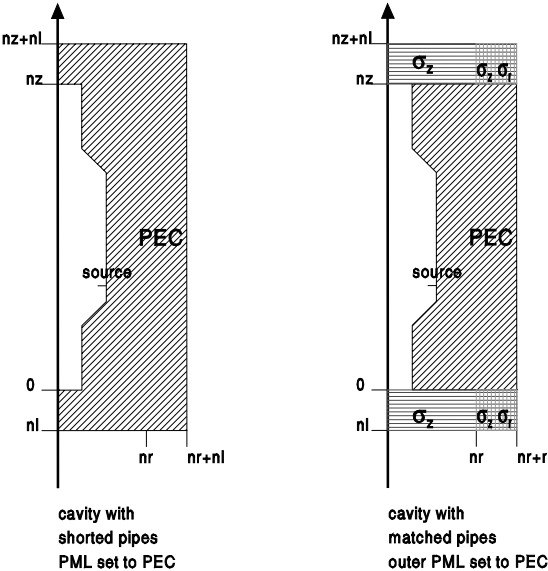**Figure 7.** Analysis of a circular patch microstrip antenna.

Figure 8. A tapered cavity for the measurement of liquids, shorted ends and matched ends.
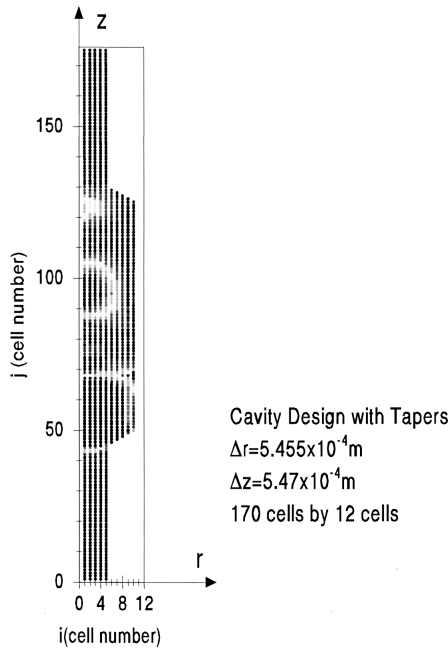
Figure 9. A tapered cavity for the measurement of properties of liquids. A plane cut of the fields (time step number 1000).

matched ends which indicates that the cavity was correctly designed such that no energy propagates down the pipes at the frequencies of interest.

5. CONCLUSIONS

Berenger's PML has been incorporated to an efficient FDTD BOR algorithm. Numerical results show that the algorithm provides results that agree with previously published data and with other numerical methods. Open resonant structures may be studied with this algorithm. Future work should concentrate on developing a near to far field transformation as was done in [3] that will provide far field quantities necessary for the study and design of the class of antennas that exhibits the BOR characteristics.
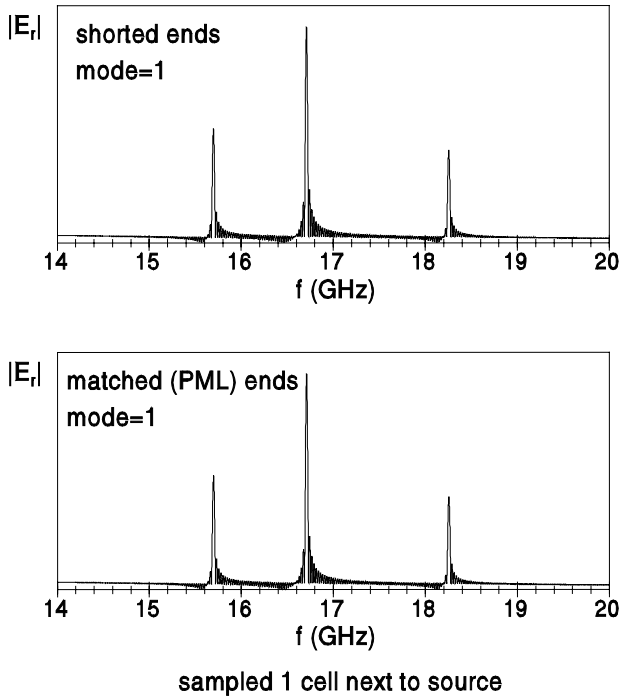
Figure 10. E_r versus frequency, for shorted and matched ends tapered cavities.

ACKNOWLEDGMENT

REFERENCES

1. Chen, Y., R. Mittra, and P. Harms, "Finite-difference time-domain algorithm for solving Maxwell's equations in rotationally symmetric geometries," *IEEE Trans. On Microwave Theory and Tech.,* Vol. MTT-44, No. 6, June 1996.
2. Kajfez, D., A. Z. Elsherbeni, and A. Mokaddem, "Higher order modes in dielectric resonators," *IEEE AP-S Antennas Propagat. Symposium,* Baltimore, Maryland, 3060–309, July 1996.

3. Maloney, J. G., G. S. Smith, and W. R. Scott, Jr., "Accurate computation of the radiation from simple antennas using the finite-difference time-domain method," *IEEE Trans. on Antennas and Prop.,* Vol. 38, No. 7, July 1994.
4. Taflove, A., *Computational Electrodynamics: The Finite Difference Time Domain Method,* Artech House, Norwood, MA, 1995.
5. Berenger, J-P., "A perfectly matched layer for the absorption of electromagnetic waves," *J. of Comp. Physics.,* No. 114, 185–200, 1994.
6. Navarro, A., and M. J. Nuñez "FDTD method coupled with FFT: A generalization to open cylindrical devices," *IEEE Trans. on Microwave Theory and Tech.,* Vol. 42, No. 5, May 1994.
7. Kishk, A. A., and S. L. Ramaraju, "Design of different configurations of finite microstrip arrays of circular patches," *Int. Journal of Microwave and Millimeter-Wave Computer-Aided Enginerring,* Vol. 4, No. 1, 6–17, 1994.
8. Kishk, A. A., M. R. Zunoubi, and D. Kajfez, "A numerical study of a dielectric disk antenna above grounded dielectric substrate," *IEEE Trans. on Antennas and Prop.,* Vol. 41, No. 6, June 1993.